Synthesis and Characterization of a Chiral, Aza-15-Crown-5-Functionalized Ferrocenyldiphosphine Ligand for Asymmetric Catalysis

Clark R. Landis,* Rachel A. Sawyer, and Ekasith Somsook

Department of Chemistry, University of Wisconsin−Madison, 1101 University Avenue, Madison, Wisconsin 53705

A chiral ferrocenyldiphosphine ligand that is functionalized with an aza crown ether, (*S*)-1-[(*R*)-1′,2-bis(diphenylphosphino)ferrocenyl]ethyl-1-aza-2,3-benzo-15-crown-5 (**1**), has been synthesized. Both the resolved and racemic ligands react rapidly with Pt(II) precursors to form stable metal−ligand adducts; the complexes PtMeI(*rac*-**1**) and PtMe₂(*rac*-**1**) have been characterized crystallographically. Reaction of *rac*-**1** with [Rh(NBD)₂]OTf yields [Rh(NBD)-(*rac*-**1**)]OTf. The three-dimensional solution structure of [Rh(NBD)(*rac*-**1**)]OTf has been determined by NOESY experiments and analysis using the two-dimensional conformer population analysis algorithm (2DCPA). The NOESY data reveal a rapid, pairwise chemical exchange between vinyl protons. The complex [Rh(NBD)(*rac*-**1**)]OTf is a catalyst precursor for hydrogenation reactions. However, we demonstrate that the lability of the aza crown ether may limit the ability of these catalysts to control selectivity via secondary interactions.

Introduction

The creation of new enantioselective, homogeneous transition-metal catalysts is the subject of intense current interest. To date, most successful enantioselective catalyst designs have focused on rigid, chiral ligands, such as the DuPHOS[1] and BINAP[2] bidentate phosphines, which impart selectivity through steric destabilization of one diastereomeric transition state. Ito and Sawamura[3] have coined the term "secondary interactions" to describe an alternate approach to designing enantioselective catalysts. Secondary interactions comprise a variety of ligand−substrate interactions, including electrostatic interactions,[4,5] hydrogen bonding,[6] and Lewis acid−base interactions.[7,8] A potential attribute of this approach is that enantiocontrol may be achieved, at least conceptually, by stabilizing one diastereomeric transition state over another. Hence, it is conceivable that secondary interactions could simultaneously increase both the rate and selectivity of a catalytic transformation. Since Ito's review[3] of secondary interactions in asymmetric catalysis, we[9,10] and others[5,11−18] have focused on the design, synthesis, and characterization of new chiral ligands containing functional groups for specific substrate complements.

Previous work in this group has involved attachment of boronato groups to an aminophenol-functionalized ferrocene ligand,[10] (*S*)-1-[(*R*)-1′,2-bis(diphenylphosphino)ferrocenyl]ethyl-2-aminophenol (BPPFAP), designed for use in Lewis acid−base and covalent secondary interactions. A single-crystal structure of a metal complex of BPPFAP, PtMeI(BPPFAP), displays the aminophenol moiety directing the N and O atoms to a position 4.0 Å above the square plane about platinum (above a coordination site that could be occupied by an incoming substrate). This indicates that the BPPFAP framework is well-suited for directing a functional group for a secondary interaction.[10] This paper focuses on the synthesis and characterization of a diphosphine ligand substituted with an aminophenol-derived crown ether. The strategy is to direct a flexible crown ether to a position above an open coordination site favorable for a secondary interaction with a functionalized substrate.

Crown ethers are known to bind ammonium cations strongly and reversibly. Binding constants of up to 10^6 M^{-1} at 25 °C have been measured for alkylammonium

(1) Burk, M. J.; Feaster, J. E.; Harlow, R. L. *Organometallics* **1990**, *9*, 2653.

(2) Noyori, R.; Takaya, H. *Acc. Chem. Res.* **1990**, *23*, 345.

(3) Sawamura, M.; Ito, Y. *Chem. Rev.* **1992**, *92*, 857.

(4) Sawamura, M.; Nagata, H.; Sakamoto, H.; Ito, Y. *J. Am. Chem. Soc.* **1992**, *114*, 2586.

(5) Sawamura, M.; Nakayama, Y.; Tang, W.; Ito, Y. *J. Org. Chem.* **1996**, *61*, 9090.

(6) Hayashi, T.; Kanehira, K.; Hagihara, T.; Kumada, M. *J. Org. Chem.* **1988**, *53*, 113.

(7) Borner, A.; Ward, J.; Kortus, K.; Kagan, H. B. *Tetrahedron: Asymmetry* **1993**, *4*, 2219.

(8) Fields, L. B.; Jacobsen, E. N. *Tetrahedron: Asymmetry* **1993**, *4*, 2229.

(9) MacFarland, D. K.; Landis, C. R. *Organometallics* **1996**, *15*, 483.

(10) Kimmich, B. F. M.; Landis, C. R. *Organometallics* **1996**, *15*, 4141.

(11) Yamazaki, A.; Achiwa, I.; Horikawa, K.; Tsurubo, M.; Achiwa, K. *Synlett* **1997**, 455.

(12) Achiwa, I.; Yamazaki, A.; Achiwa, K. *Synlett* **1998**, 45.

(13) Komarov, I.; Gorichko, M. V.; Kornilov, M. Y. *Tetrahedron: Asymmetry* **1997**, *8*, 435.

(14) Heller, D.; Holz, J.; Borns, S.; Spannenberg, A.; Kempe, R.; Schmidt, U.; Borner, A. *Tetrahedron: Asymmetry* **1997**, *8*, 213.

(15) Yamada, I.; Yamaguchi, M.; Yamagishi, T. *Tetrahedron: Asymmetry* **1996**, *7*, 3339.

(16) Yamada, I.; Fukui, K.; Aoki, Y.; Ikeda, S.; Yamaguchi, M.; Yamagishi, T. *J. Organomet. Chem.* **1997**, *539*, 115.

(17) Jiang, Y.; Jiang, Q.; Zhang, X. *J. Am. Chem. Soc.* **1998**, *120*, 3817.

(18) Jiang, Y.; Jiang, Q.; Zhu, G.; Zhang, X. *Tetrahedron Lett.* **1997**, *38*, 6565.

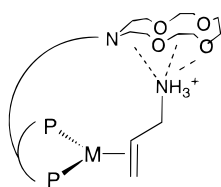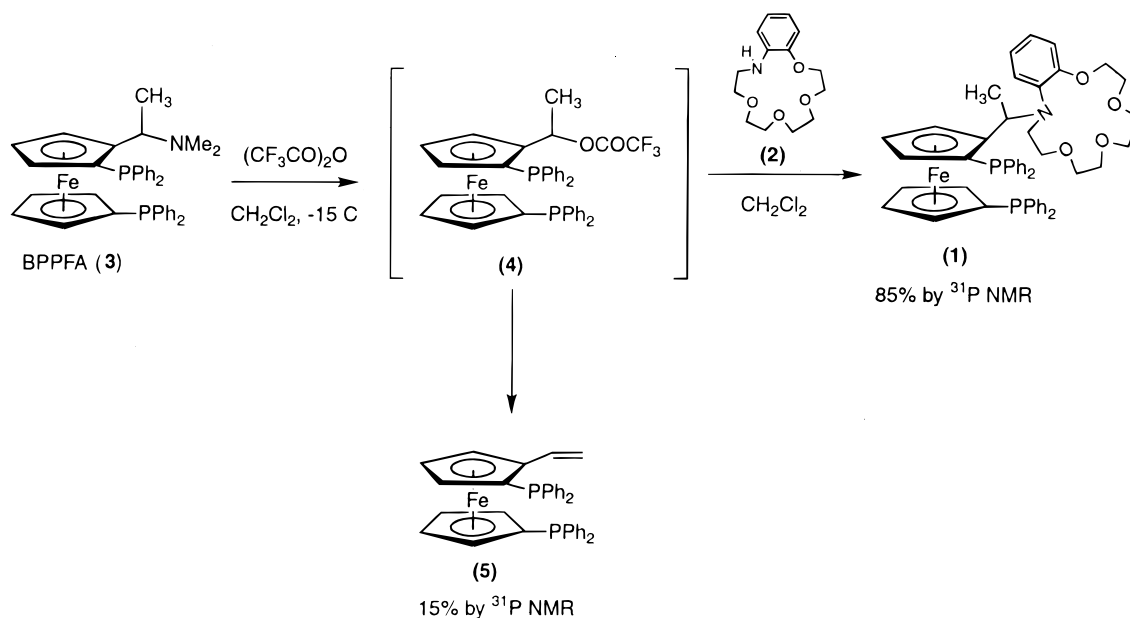**Scheme 1. Synthesis of 1**

Figure 1. Proposed hydrogen-bonding secondary interaction between a crown ether and an alkylammonium cation.

cations.[19] We seek to exploit this hydrogen-bonding interaction between a crown ether and an ammonium cation for the creation of a selectivity-directing secondary interaction (Figure 1). Ito[4,5] previously has synthesized crown ether functionalized ligands focusing on an electrostatic interaction between an encapsulated metal cation and a negatively charged substrate. This group also has synthesized chiral crown ether diphosphite ligands designed for a similar hydrogen-bonding interaction.[9]

Results and Discussion

Chiral ferrocenylphosphines are easily substituted at the α position using (S)-1-[(R)-1′,2-bis(diphenylphosphino)ferrocenyl]ethyl acetate (BPPFAc)[20] as a starting material. Hayashi and co-workers,[20,21] Landis and co-workers,[10] and others[22] have achieved a variety of side chain substitutions using this method. Attempts at using this route for the target ligand, (S)-1-[(R)-1′,2-bis-(diphenylphosphino)ferrocenyl]ethyl-1-aza-2,3-benzo-15-crown-5 (**1**), in a variety of solvents, as well as the neat reaction in a melt of the aza crown ether (100 °C, excess 1-aza-2,3-benzo-15-crown-5 (**2**)), failed. Previously Ugi

and co-workers[23] have formed substituted ferrocenes by displacing an ammonium group from the α-position. However, Hayashi[20] found that for ferrocenyl *phosphine* (S)-N,N-dimethyl-1-[(R)-2-(diphenylphosphino)ferrocenyl]ethylamine (PPFA) the phosphonium cation was formed preferentially over the desired ammonium cation. Protection of the phosphine by conversion to the phosphine oxide allowed for the substitution. Hayashi's method involves additional protection and deprotection steps; therefore, a more convenient route was desired. Replacing the acetate leaving group with the more reactive trifluoroacetate leaving group yielded the target ligand **1**.

Reaction of 1 equiv of trifluoroacetic anhydride with (S)-N,N-dimethyl-1-[(R)-1′,2-bis(diphenylphosphino)ferrocenyl]ethylamine (**3**, BPPFA)[20] resulted in a single product that had characteristic ^{1}H and ^{31}P NMR peaks similar to those of BPPFAc. This product could not be isolated, as it rapidly eliminates trifluoroacetic acid to yield the vinylferrocenylphosphine **5**. Sequential addition of trifluoroacetic anhydride and the crown nucleophile (**2**) to BPPFA in CH_2Cl_2 at −15 °C produced **1** in good yield (Scheme 1). Column chromatography gave the pure ligand as a yellow powder. The ligand was synthesized in both resolved and racemic forms using this method. This new synthetic route eliminates an isolation step and provides a convenient method that can be applied to obtain a variety of functionalized ferrocene ligands.

The racemic ligand **1** was characterized using ^{1}H and ^{31}P NMR, elemental analysis, and LSIMS mass spectroscopy. The phosphine resonances at −17.3 and −25.8 ppm are consistent with similar ferrocene ligands made by this group[10] and others.[20] The ^{1}H NMR spectrum displays resonances that are characteristic of this class of ferrocene ligands; most diagnostic are the methyl and methine resonances associated with the α-carbon of the substituted cyclopentadienyl group.

Further characterization of the ligand *rac*-**1** was achieved by its reaction with a series of metal com-

(19) Inoue, Y.; Gokel, G. W. *Cation Binding by Macrocycles*; Marcel Dekker: New York, 1990.

(20) Hayashi, T.; Mise, T.; Fukushima, M.; Kagotani, M.; Nagashima, N.; Hamada, Y.; Akira, M.; Kagotani, S.; Konishi, M.; Yamamoto, K.; Kumada, M. *Bull. Chem. Soc. Jpn.* **1980**, *53*, 1138.

(21) Sawamura, M.; Kitayama, K.; Ito, Y. *Tetrahedron: Asymmetry* **1993**, *4*, 1829.

(22) Yamazaki, A.; Morimoto, T.; Achiwa, K. *Tetrahedron: Asymmetry* **1993**, *4*, 2287.

(23) Ugi, I. K.; Gokel, G. W. *J. Chem. Educ.* **1972**, *49*, 294.

Scheme 2. Preparation of Platinum Complexes of *rac*-1

6 $R_1=R_2=Me$
7 $R_1=R_2=Cl$
8a $R_1=Me$, $R_2=I$
8b $R_1=I$, $R_2=Me$
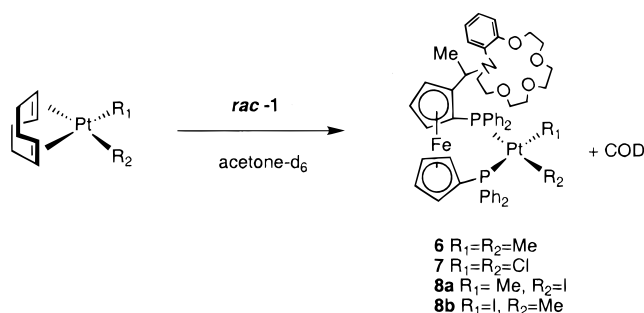
Table 1. Selected Bond Lengths (Å) and Bond Angles (deg) for PtMeI(*rac*-1)

Bond Lengths			
Pt(1)−C(56)	2.109(4)	P(2)−Pt(1)	2.2891(10)
Pt(1)−I(1)	2.5835(5)	N(37)−C(35)	1.488(5)
P(1)−Pt(1)	2.3002(11)		

Bond Angles			
C(56)−Pt(1)−I(1)	84.0(3)	P(1)−Pt(1)−I(1)	94.47(3)
P(1)−Pt(1)−P(2)	98.49(3)	P(2)−Pt(1)−C(56)	82.5(3)

Table 2. Crystallographic Data for PtMeI(*rac*-1)

formula	$C_{51}H_{54}FeINO_4P_2Pt$
fw	1184.73
cryst color, habit	yellow transparent prism
cryst size, mm	0.34 × 0.22 × 0.18
cryst syst	triclinic
space group	$P\bar{1}$
a, Å	12.4278(5)
b, Å	13.5881(6)
c, Å	14.9499(7)
β, deg	65.940
V, Å³	2297.6(2)
Z	2
ρ_{calcd}, g cm⁻³	1.712
T, K	133(2)
$F(000)$	1172
radiation; λ, Å	Mo Kα; 0.710 73
diffractometer	Siemens P4/CCD
2θ(max), deg	58.34
no. of rflns collected	26213
no. of rflns used	9805
no. of params refined	561
R, $I > 2\sigma(I)$	0.0393
R_w	0.0775
goodness of fit on F^2	1.158

plexes. The diphosphine *rac*-**1** was reacted with PtMe₂-COD, PtMeICOD, and PtCl₂COD to form the ligand complexes **6**−**8** (Scheme 2). These reaction products were characterized by ³¹P and ¹H NMR spectroscopy, elemental analysis, and, for **6** and **8**, X-ray crystallography. Ligation of the added diphosphine was indicated by the appearance of free COD resonances in the ¹H NMR. ³¹P NMR also indicated formation of the metal complexes, revealing characteristic platinum coupling patterns[10] and coupling between the inequivalent phosphorus atoms.

Diphosphine *rac*-**1** reacted with PtMeI(COD) in acetone to form a yellow solid. The ¹H and ³¹P NMR spectra, elemental analysis, and the single-crystal structure (Tables 1 and 2, Figure 2) are all consistent with the formulation PtMeI(*rac*-**1**). Because the phosphorus atoms are inequivalent, two geometric isomers are formed; the major isomer is **8b**. In solution these isomers are present in a 60:40 ratio, as shown by ³¹P NMR. A single-crystal structure showed the Me and I
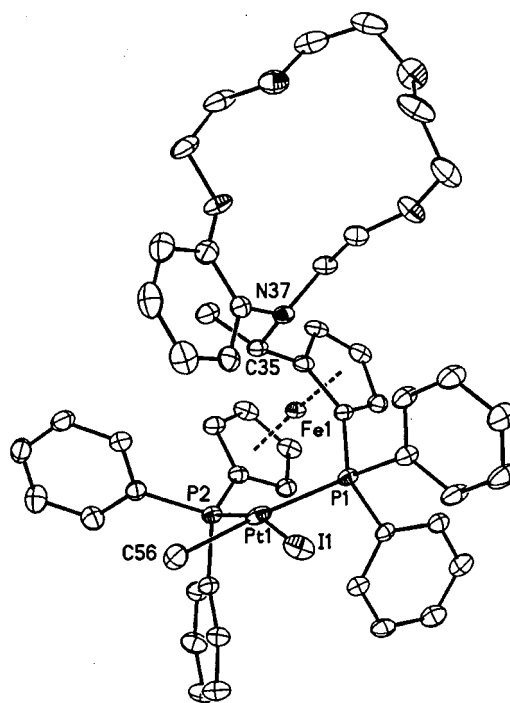

Figure 2. X-ray crystal structure for PtMeI(*rac*-**1**) (**8a**). The displacement ellipsoids are drawn at 50% probability. Hydrogens have been removed for clarity.

groups bonded to platinum to be disordered and the mixture of isomers to be essentially 50:50. The coordination geometry about the Pt atom is distorted square planar (the angle values range from 82.5(3) to 98.49-(3)°). The ferrocene moiety shows the characteristic tilt, with the centers of both rings above the approximate square plane about platinum. The phosphorus−platinum bond lengths (2.3002(11) and 2.2891(10) Å) of PtMeI(*rac*-**1**) are very similar to those of PtMeI(BPP-FAP)[10] (2.3215(10) and 2.2737(10) Å).

Unfortunately, the single-crystal structure of PtMeI-(*rac*-**1**) revealed that the crown ether moiety was twisted away from the Pt center, unlike the aminophenol group in the structure of PtMeI(BPPFAP),[10] for which the plane of the aminophenol moiety cantilevers above, and nearly parallel to, the Pt coordination plane. Rotation about the C35−N37 bond and a twist of the crown ether ring would allow the ligand to achieve a structure that would be more favorable to a secondary interaction. Such motion may be freely available in solution (vide infra). A longer alkyl "tether" between the ferrocenyl rings and the crown ether would allow more conformational flexibility for positioning of the crown ether. Currently it is not known whether this flexibility would be beneficial or not.

The single-crystal X-ray structure of PtMe₂(*rac*-**1**) is similar to that of PtMeI(*rac*-**1**). The crystal data are summarized in the Supporting Information.

Reaction of *rac*-**1** with [Rh(NBD)₂]OTf in acetone led to the formation of [Rh(NBD)(*rac*-**1**)]OTf (**9**), as indicated by ¹H and ³¹P NMR spectra (Scheme 3). Formation of the rhodium complex was supported by the appearance of free norbornadiene resonances in the ¹H NMR spectrum and by coupling to rhodium ($I = \frac{1}{2}$) in the ³¹P NMR spectrum (J_{P-Rh} = 160 and 162 Hz). Coupling between the inequivalent phosphorus atoms was also seen (J_{P-P} = 26 Hz). This complex decomposed with loss

Scheme 3.   Preparation of [Rh(NBD)(*rac*-1)]OTf (9)
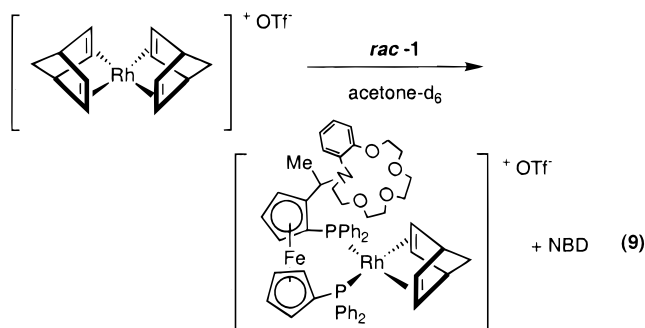
Scheme 4.   Reaction of *rac*-1 with Allylammonium Triflate
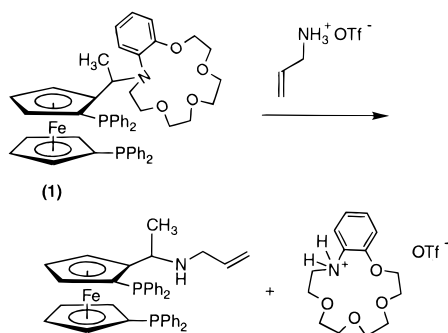
of the crown ether over a period of weeks in acetone solution, presumably due to slow hydrolysis at the α-carbon.

Rhodium complexes of **1** are catalysts for the hydrogenation of simple substrates. Quantitative hydrogenation of methyl (*Z*)-α-acetamidocinnamate, MAC, was observed with the rhodium complex of **1** generated in situ from [Rh(NBD)₂]OTf and *rac*-**1**. Hydrogenation of MAC using resolved ligands gave unremarkable enantiomeric excesses, 79% ee for (*S*,*R*)-**1** compared to 69% ee for (*S*,*R*)-BPPFA under similar conditions. Preliminary rate measurements show the rate of hydrogenation of MAC with [Rh(NBD)(*rac*-**1**)]OTf is slightly faster (3585 turnovers/h) than with a control catalyst, [Rh-(NBD)(*rac*-BPPFA)]OTf (1651 turnovers/h). An attempt to probe the possible kinetic acceleration of hydrogenation due to secondary interactions with the crown ether functional group was thwarted by an unexpectedly facile substitution reaction. Under catalytic conditions, the hydrogenation of allylammonium triflate as catalyzed [Rh(NBD)(*rac*-**1**)]OTf exhibited erratic kinetic behavior with very fast initial rates of hydrogen uptake that slowed substantially during the first few minutes of reaction before more than 5% of the substrate had been consumed. Subsequent studies of the reaction of allylammonium triflate with **1** revealed that a rapid substitution reaction takes place in which allylamine substitutes for the aza crown ether (Scheme 4).

Solution Structure Determination of [Rh(NBD)-(*rac*-1)]OTf (9) by Two-Dimensional Conformer Population Analysis (2DCPA). The conformations of molecules in the solid state may differ from those in solution, particularly for conformers differing only in torsion angles. In the case of the Pt complex **8a** we hypothesized that the undesired crystallographic conformation could revert to the desired conformation in
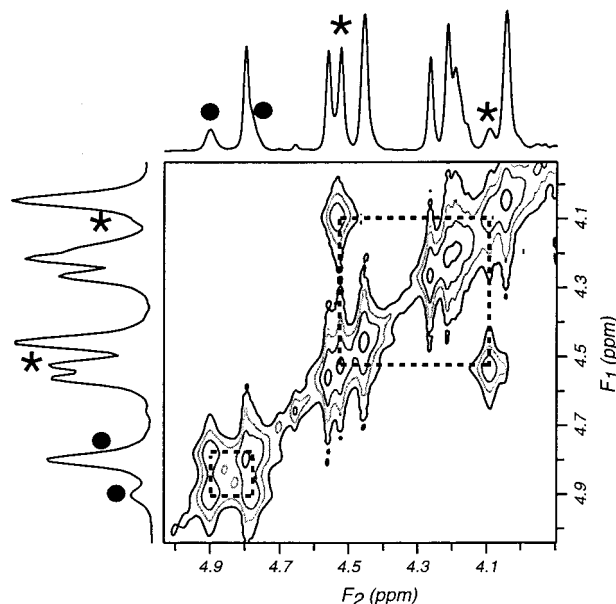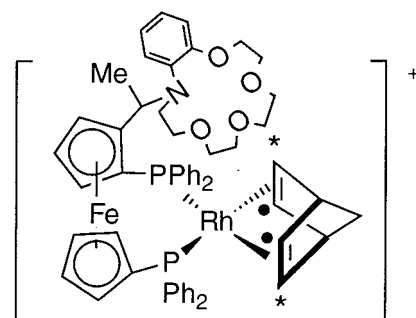

Figure 3. Contour plot of the 2DNOESY spectrum of [Rh-(NBD)(*rac*-**1**)](OTf) in *d*₆-acetone at 24 °C demonstrating pairwise chemical exchange between vinyl protons (NOE cross-peaks are of opposite sign and are not shown in this spectrum).

solution via rotation about the C35−N37 bond and twisting of the crown ether. This led us to investigate the solution structures of [Rh(NBD)(*rac*-**1**)]OTf (**9**) through analysis of the time course of the quantitative ¹H 2D NOESY data with the multiconformational analysis technique, two-dimensional conformation population analysis (2DCPA).[24−29] This complex was chosen for solution structure analysis because the norbornadiene ligand leads to a richer set of NOE cross-peaks than would be seen for the Pt complex **8a**.

2DCPA analysis correlates the observed NOESY intensities (or, alternatively, the experimental cross-relaxation rates) at each mixing time to the calculated NOE data from a set of energetically reasonable trial models created by molecular mechanics. In contrast to

(24) Casey, C. P.; Hallenbeck, S. L.; Wright, J. M.; Landis, C. R. *J. Am. Chem. Soc.* **1997**, *119*, 9680.
(25) Giovannetti, J. S.; Kelly, C. M.; Landis, C. R. *J. Am. Chem. Soc.* **1993**, *115*, 4040.
(26) Kimmich, B. F. M.; Somsook, E.; Landis, C. R. *J. Am. Chem. Soc.* **1998**, *120*, 10115.
(27) Landis, C. R.; Allured, V. S. *J. Am. Chem. Soc.* **1991**, *113*, 9493.
(28) Landis, C. R.; Luck, L. L.; Wright, J. M. *J. Magn. Reson., Ser. B* **1995**, *109*, 44.
(29) Wright, J. M.; Landis, C. R.; Ros, M. A. M. P.; Horton, A. D. *Organometallics* **1998**, *17*, 5031.

Scheme 5. Three Plausible Mechanisms of Vinyl Group Chemical Exchange: (1) NBD Rotation via a Squashed Tetrahedral Transition State, (2) Solvent Association Leading to a Trigonal Bipyramidal Transition State or Intermediate, and (3) Intramolecular Crown Ether Coordination Leading to a Trigonal Bipyramidal Transition State or Intermediate
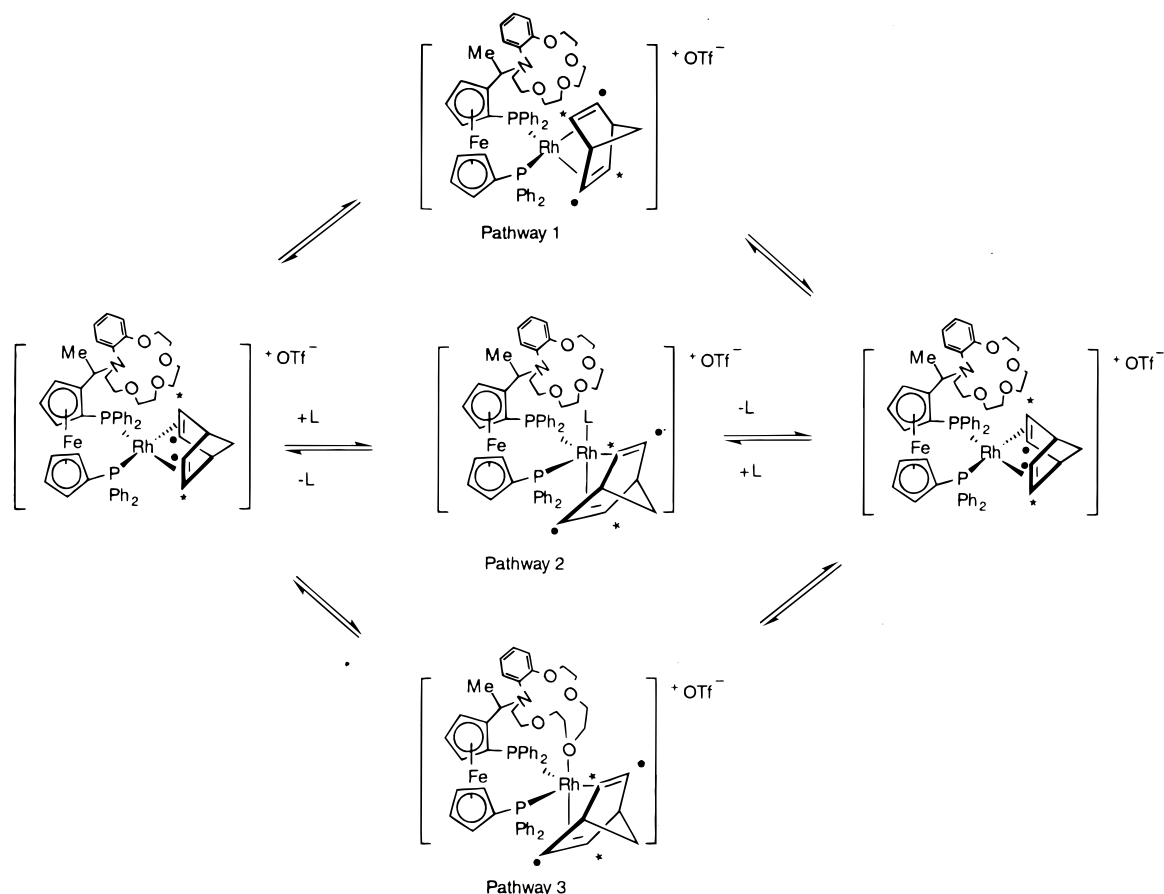
the single, average solution structure approach, 2DCPA yields the smallest combination of statistically significant conformers and their populations. Our analysis involved three steps: (1) collection of NOESY time courses, (2) creation of an ensemble of trial conformers using molecular mechanics, and (3) conformer population analysis of the observed NOESY time courses. The NOESY data collected in acetone-d_6 at 24 °C (mixing times of 300, 450, 600, 900, and 1200 ms) resulted in positive NOE's (see the Supporting Information).

The NOESY spectrum of **9** reveals an interesting chemical exchange process that interconverts two pairs of NBD vinyl protons (Figure 3). The cross-peaks arising from chemical exchange have phase opposite to that of NOE cross-peaks and are readily identified. The mechanism of exchange does not involve complete dissociation/reassociation of the NBD ligand. The chemical exchange process requires that at least one alkene remain coordinated throughout the exchange process; otherwise, exchange among all of the vinyl NBD peaks would be seen. The simplest process that will yield the observed exchange pattern is rotation of the NBD ligand at the metal center via a squashed tetrahedral transition state (Scheme 5). Alternative mechanisms involve coordination of either solvent or the crown ether to yield a five-coordinate intermediate or transition state which can revert back to the four-coordinate square planar complex with rotation of the NBD group in either of two directions. The kinetics of the chemical exchange process

were measured by magnetization transfer using the 1D DPFGSE-NOE experiments[30,31] at several temperatures. These experiments yield an enthalpy of activation of 8.7 kcal/mol and a 25 cal/(mol K) entropy of activation. The details of calculations concerning chemical exchange in the solution structures and 1D DPFGSE-NOE experiments are described in the Experimental Section.

The goal of the quantitative analysis of the NOE data is to determine whether structures suitable to the secondary interactions are significantly populated in solution. The primary conformational degree of freedom corresponds to the twisting along the bond of C35−N37. Quantitative analysis of the NOE time courses finds that the most populated conformer has the crown ether moiety away from the metal site, similar to the crystallographic conformation of PtMeI(*rac*-**1**) (**8a**), whereas the less populated conformers have the crown ether close to the metal center. The fit to the observed data using two or three conformers yields a statistically significant better fit than using a single conformer. This result indicates that more than one conformation of the complex is required to simulate the NOE time course. The two best-fit conformers are shown in Figure 4. The 2DCPA method does not use molecular mechanics energies in finding the conformers that best satisfy the

(30) Stonehouse, J.; Adell, P.; Keeler, J.; Shaka, A. J. *J. Am. Chem. Soc.* **1994**, *116*, 6037.
(31) Stott, K.; Keeler, J.; Van, Q. N.; Shaka, A. J. *J. Magn. Reson.* **1997**, *125*, 302.
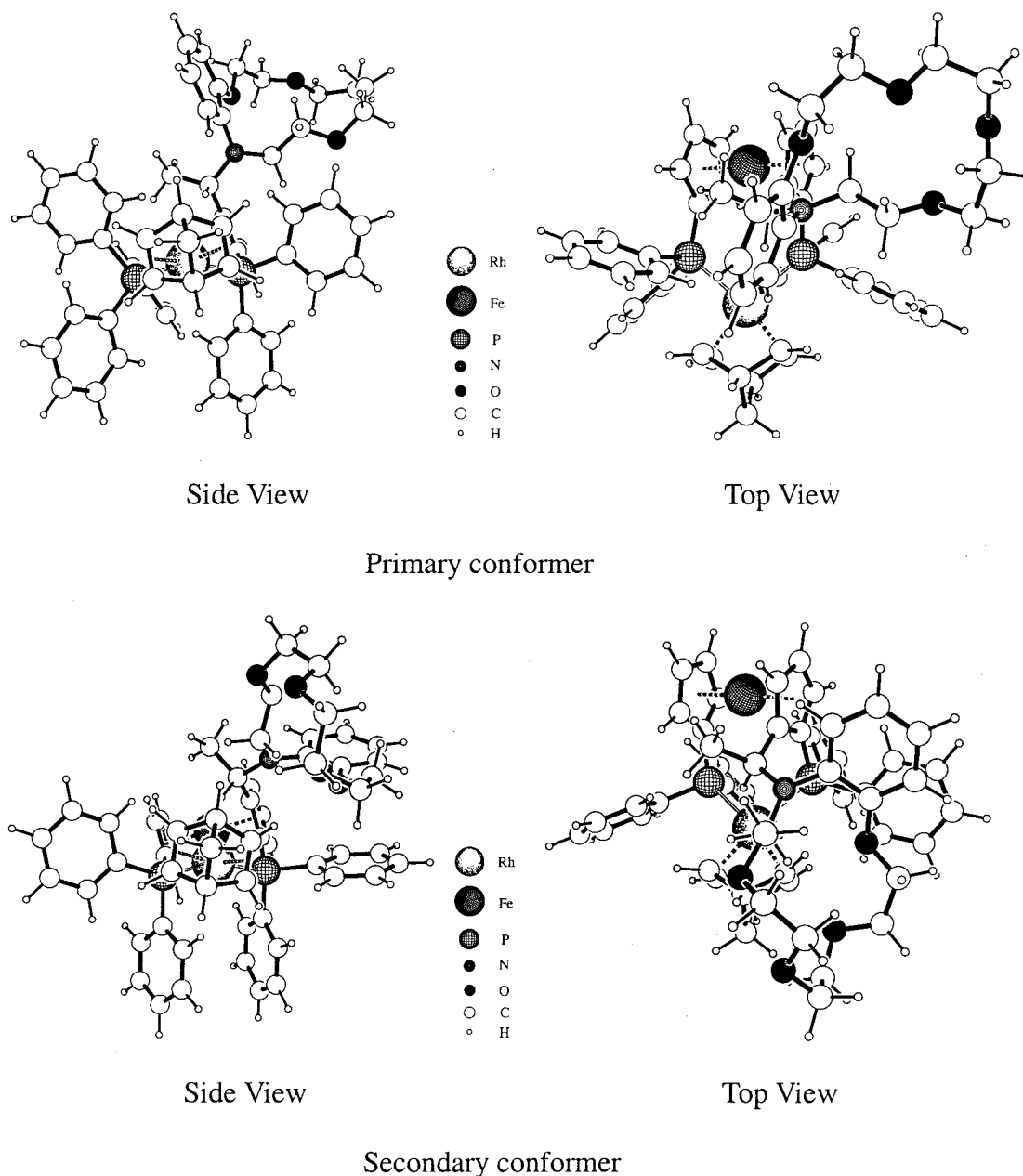
Side View

Top View

Primary conformer

Side View

Top View

Secondary conformer

Figure 4. The two best-fit conformers from 2DCPA in side view and top view.

Table 3. Energies (kcal/mol) and Torsion Angles (deg) of the Best-Fit Conformers

conformer	molecular mechanics energy	torsion angle	
		Me−C35−N37−C_{ipso}	C15(Fc)−C14(Fc)−C35−Me
primary	244	165	−128
secondary	245	16	−149
tertiary	265	−47	−8

empirical NOE data. On the basis of molecular mechanics calculations with the UFF force field, the primary, secondary, and tertiary conformers have energies within 9, 9, and 29 kcal/mol of the lowest energy conformation, respectively (see Table 3). The total conformational space represented in the molecular mechanics ensemble is represented in Figure 5.

Conclusions

The new benzo-aza crown ether functionalized ferrocenylphosphine **1** has been prepared. This ligand reacts
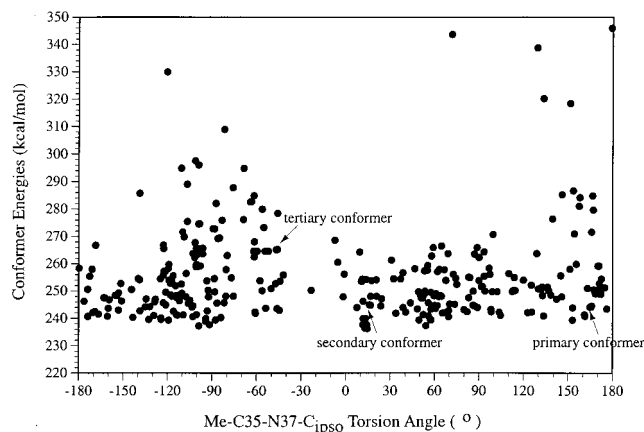
Figure 5. Distribution of conformer energies obtained from molecular mechanics computations.

with a series of platinum and rhodium complexes in a manner similar to that for other diphosphine ligands.

The crystallographic structure of the complex Pt(**1**)MeI reveals a near-equal distribution between two geometric isomers and an orientation of the crown ether that would not support secondary interactions. However, the structures of [Rh(**1**)(NBD)](OTf) in acetone *solution*, which were determined by multiconformational analysis of the NOESY time course, support some population of conformations in which the benzo-aza crown ether is capable of engendering secondary interactions. Although the complex [Rh(**1**)(NBD)](OTf) is an active hydrogenation catalyst for simple olefins, attempts to effect strong secondary interactions with allylammonium substrates were complicated by substitution of the benzo-aza crown ether by allylamine.

Experimental Section

General Procedures. All manipulations of air-sensitive compounds were done under nitrogen using either standard Schlenk techniques or an inert-atmosphere glovebox. All solvents were distilled under nitrogen using standard drying techniques. ^{1}H NMR (300 MHz) and ^{31}P{^{1}H} NMR (121 MHz) spectra were performed on a Bruker AC-300 spectrometer. ^{1}H spectra were referenced to TMS and ^{31}P spectra to an external H_3PO_4 standard. LSIMS mass spectra were recorded with a VG AutoSpec spectrometer. Elemental analyses was performed by Desert Analytics Laboratory. Optical rotations were measured on a Perkin-Elmer 241 Polarimeter. All GC runs were performed on a HP5890A gas chromatograph using an Alltech Chirasil-Val column. The compounds 1,12-dichloro-3,6,9-trioxaundecane,[32] (*S,R*)-BPPFA,[20] PtMe$_2$(COD),[33] PtMeI(COD),[33] PtCl$_2$(COD),[33] and [Rh(NBD)$_2$]OTf[34] were synthesized according to literature procedures. All other reagents were purchased from Aldrich and used as received.

1-Aza-2,3-benzo-15-crown-5 (2). The procedure for the preparation of **2** was based on a procedure by Pedersen.[32] 2-Aminophenol (29.6 g, 0.271 mol) and 1,12-dichloro-3,6,9-trioxaundecane (62.5 g, 0.269 mol) were refluxed in *n*-butyl alcohol for 18 h under N$_2$. The reaction mixture was cooled to 65 °C, and a solution of 25 g of sodium hydroxide in 25 mL of water was added. The resulting mixture was refluxed for 10 h. The warm reaction mixture was filtered and the solvent removed to yield a brown oil. The oil was dissolved in chloroform and the solution washed with 5% NaOH(aq) (3 × 20 mL). The chloroform layer was dried over MgSO$_4$ and the solvent removed. The resulting brown oil was distilled under vacuum at high temperatures (>200 °C) to give a white solid. The solid was recrystallized in *n*-heptane, yielding white crystals (5.69 g). Yield: 8%. Data: ^{1}H NMR (CDCl$_3$) δ 3.24 (s, broad 2H, HNC*H*$_2$), 3.69 (m, 8H, C*H*$_2$C*H*$_2$OC*H*$_2$C*H*$_2$), 3.78 (t, 2H, HNCH$_2$C*H*$_2$), 3.84 (m, 2H, PhOCH$_2$C*H*$_2$), 4.10 (m, 2H, PhOC*H*$_2$), 5.13 (s, broad Hz, 1H, *H*NCH$_2$), 6.57 (dd, *J* = 7.72, 1.47 Hz, 1H, Ph *H*), 6.61 (td, *J* = 7.72, 1.47 Hz, 1H, Ph *H*), 6.75 (dd, *J* = 7.72, 1.47 Hz, 1H, Ph *H*), 6.86 (td, *J* = 7.72, 1.47 Hz, 1H, Ph *H*); ^{13}C NMR (CDCl$_3$) δ 43.20, 68.24, 69.00, 69.53, 69.92, 70.03 (2C), 70.40, 110.24, 111.90, 116.30, 121.81, 139.52, 146.36; EI MS m$^+$ *m/e* 267.3.

(*S,R*)-1. (*S,R*)-BPPFA (0.62 g, 0.99 mmol) was placed in a Schlenk flask under N$_2$. Trifluoroacetic anhydride (2.5 mL of a 0.4 M solution in CH$_2$Cl$_2$) was added at −15 °C. Immediately afterward, a solution of 1-aza-2,3-benzo-15-crown-5 (0.28 g, 1.1 mmol) and triethylamine (0.15 mL, 1.1 mmol) in 3 mL of CH$_2$-Cl$_2$ was added. The solution was stirred at −15 °C for 1 h, warmed to room temperature, and stirred at room temperature

for 18 h. The solvent was removed, and degassed benzene was added. The solution was washed with water, and the water layer was extracted with benzene (3 × 10 mL). The combined benzene layers were dried over Na$_2$SO$_4$. The solvent was removed, yielding an orange oil. The oil was chromatographed on silica using hexane/CH$_2$Cl$_2$/triethylamine as the eluent. The fractions containing the product were combined and the solvent reduced. The product crystallized as a yellow powder (0.266 g). Yield: 30%. Data: [α]^{25}$_D$ = +275 (CHCl$_3$, *c* 1.57); ^{1}H NMR (CDCl$_3$) δ 1.42 (d, *J* = 6.62 Hz, 3H, CHC*H*$_3$), 2.38 (m, 1H, PhNC*H*$_2$), 2.80 (td, *J* = 10.80, 4.41 Hz, 1H, PhNC*H*$_2$), 2.96 (m, 1H, NCH$_2$C*H*$_2$), 3.24 (m, 1H, OC*H*$_2$), 3.30 (m, 1H, NCH$_2$C*H*$_2$), 3.4−4.0 (m, 14H, C$_5$*H*$_4$, C$_5$*H*$_3$, and OC*H*$_2$), 4.07 (m, 2H, C$_5$*H*$_4$ and C$_5$*H*$_3$), 4.30 (s, 1H, C$_5$*H*$_4$ or C$_5$*H*$_3$), 4.51 (s, 1H, C$_5$*H*$_4$ or C$_5$*H*$_3$), 4.80 (qd, *J* = 6.62, 2.57 Hz, 1H, CH$_3$C*H*N), 6.65 (dd, *J* = 8.09, 1.47 Hz, 1H, Ph *H*), 6.79 (td, *J* = 7.54, 1.10 Hz, 1H, Ph *H*), 6.87 (td, *J* = 7.67, 1.47 Hz, 1H, Ph *H*), 7.1−7.5 (m, 21H, (C$_6$*H*$_5$)$_2$P and Ph *H*); ^{31}P NMR (CDCl$_3$) δ −17.3 (s, (C$_6$H$_5$)$_2$*P*), −25.8 (s, (C$_6$H$_5$)$_2$*P*); LR LSIMS MS m$^+$ *m/e* 847.26. Anal. Calcd for C$_{50}$H$_{51}$NO$_4$P$_2$Fe: C, 70.83; H, 6.06; N, 1.65; P, 7.31; Fe, 6.59. Found: C, 70.74; H, 6.26; N, 1.70; P, 6.05; Fe, 6.95.

Reaction of PtMe$_2$(COD) with *rac*-1. A solution of crude *rac*-**1** (25.4 mg, 60% **1**, 8% **5**, 50% **2** by NMR, 1.80 × 10$^{−2}$ mmol) in 0.5 mL of *d$_6$*-acetone was added to a solution of PtMe$_2$(COD) (10.0 mg, 3.03 × 10$^{−2}$ mmol) in 0.5 mL of *d$_6$*-acetone under nitrogen. Yellow crystals result from slow evaporation of solvent in a warm water bath. Data: ^{1}H NMR (*d$_6$*-acetone) δ 0.25 (ddd, 3H, $J_{H−Pt}$ = 35 Hz, $J_{H−P}$ = 9 Hz, $J_{H−P}$ = 9 Hz, PtC*H*$_3$), 0.60 (ddd, 3H, PtC*H*$_3$), 1.38 (d, 3H, $J_{H−H}$ = 6.9 Hz, C*H*$_3$), 2.31 (m, H), 3.20 (m, 2H, C*H*$_2$O), 3.42 (m, 2H, C*H*$_2$O), 3.45−3.70 (m, many H, CH$_2$O and Cp), 3.90 (m, 2H, CH$_2$O or Cp or vinyl COD), 4.05 (m, 2H, CH$_2$O or Cp or vinyl COD), 4.15 (m, 2H, CH$_2$O or Cp or vinyl COD), 4.20 (m, 1H, CH$_2$O or Cp or vinyl COD), 4.25 (m, 2H, CH$_2$O or Cp or vinyl COD), 4.28 (m, 2H, CH$_2$O or Cp or vinyl COD), 4.55 (m, 1H, CH$_2$O or Cp or vinyl COD), 5.50 (m, 2H, CH$_2$O or Cp or vinyl COD), 6.03 (q, 1H, *J* = 6.9 Hz, CH), 6.60−6.97 (m, 4H, C$_6$*H*$_4$), 7.04−8.05 (m, 20H, PPh$_2$); ^{31}P NMR (*d$_6$*-acetone) δ 21.7 (dd, $J_{P−Pt}$ = 1880 Hz, $J_{P−P}$ = 13 Hz), 27.4 (dd, $J_{P−Pt}$ = 1964 Hz, $J_{P−P}$ = 13 Hz). Anal. Calcd for C$_{52}$H$_{57}$NO$_4$P$_2$FePt: C, 58.10; H, 5.34; N, 1.30. Found: C, 57.85; H, 5.21; N, 1.42.

Reaction of PtCl$_2$(COD) with *rac*-1. A solution of *rac*-**1** (10.8 mg, 0.013 mmol) in 0.5 mL of acetone was added dropwise to a solution of PtCl$_2$(COD) (10.0 mg, 0.026 mmol) in 0.5 mL of acetone. A pale yellow solid immediately precipitated. The acetone was poured off, and the solid was dried in vacuo. Repeated elemental analyses of different batches of this material yielded significantly different results (e.g., % C varied ±3%), presumably due to differing amounts of solvent impurities. Data: ^{1}H NMR (CD$_2$Cl$_2$) δ 1.37 (d, *J* = 7 Hz, 3H, CHC*H*$_3$), 3.2−4.5 (m, 23H, C*H*$_2$N, C*H*$_2$O, and C$_5$*H*$_3$FeC$_5$*H*$_4$), 6.77 (t, *J* = 7 Hz, 1H, C*H*CH$_3$), 6.85−8.25 (m, 24H, C$_6$*H*$_4$NO and PC$_6$*H*$_5$); ^{31}P NMR (CD$_2$Cl$_2$) δ 17.8 (dd, $J_{P−Pt}$ = 3826 Hz, $J_{P−P}$ = 10 Hz), 12.03 (dd, $J_{P−Pt}$ = 3748 Hz, $J_{P−P}$ = 10 Hz). Anal. Calcd for C$_{50}$H$_{51}$NO$_4$P$_2$FeCl$_2$Pt: C, 53.82; H, 4.61; N, 1.26. Found (best): C, 52.10; H, 4.37; N, 1.50.

Reaction of PtMeI(COD) with *rac*-1. PtMeI(COD) (49.3 mg, 0.11 mmol) and *rac*-**1** (97.0 mg, 0.12 mmol) were placed in a Schlenk flask under nitrogen. Acetone (10 mL) was added. The solution was stirred for 1 h. A yellow powder precipitated. [PtMeI(**rac*-1**)] was found to be a 60:40 mixture of two isomers by ^{31}P NMR. Data: ^{1}H NMR (CD$_2$Cl$_2$) δ 0.43 (tt, $J_{Pt−H}$ = 30 Hz, $J_{P−H}$ = 7 Hz, 3H, PtC*H*$_3$ (minor)), 1.10 (tt, $J_{Pt−H}$ = 30 Hz, $J_{P−H}$ = 7 Hz, 3H, PtC*H*$_3$ (major)), 1.25 (d, *J* = 7 Hz, 3H, CHC*H*$_3$ (major)), 1.57 (d, *J* = 7 Hz, 3H, CHC*H*$_3$ (minor)), 3.20−4.78 (m, 46H, CH$_2$N, CH$_2$O, and C$_5$H$_3$FeC$_5$H$_4$ from both major and minor), 6.70−8.27 (m, 25H, C*H*CH$_3$, C$_6$*H*$_4$NO, and PC$_6$*H*$_5$); ^{31}P NMR (CD$_2$Cl$_2$) **8a**, δ 22.1 (dd, $J_{P−Pt}$ = 4327 Hz, $J_{P−P}$ = 13 Hz), 16.9 (dd, $J_{P−Pt}$ = 1781 Hz, $J_{P−P}$ = 13 Hz); ^{31}P NMR (CD$_2$Cl$_2$) **8b**. δ 23.7 (dd, $J_{P−Pt}$ = 1950 Hz, $J_{P−P}$ = 13 Hz), 18.9 (dd, $J_{P−Pt}$

(32) Pedersen, C. J. *J. Am. Chem. Soc.* **1967**, *89*, 7017.

(33) Clark, H. C.; Manzer, L. E. *J. Organomet. Chem.* **1973**, *59*, 411−428.

(34) Abel, E. W.; Bennett, M. A.; Wilkinson, G. *J. Chem. Soc.* **1959**, 3178.

= 4357 Hz, J_{P-P} = 13 Hz). Anal. Calcd for $C_{51}H_{54}NO_4P_2FeIPt$: C, 51.61; H, 4.59; N, 1.18. Found: C, 51.89; H, 5.33; N, 1.00.

Structure Determination of PtMeI(*rac*-1). Single crystals were grown from acetone-d_6 at room temperature. The crystal data are summarized in Table 2.

A total of 26 213 reflections with 2θ < 58° was collected on a Siemens P4/CCD diffractometer using graphite-monochromated Mo Kα radiation.[35,36] The structure was solved by direct methods and refined by full-matrix least squares on F^2 values with hydrogens riding.[37] Non-hydrogen atoms were refined with anisotropic displacement parameters. The final R and R_w factors were 0.0393 and 0.0775, respectively, for 9805 reflections (I < $2\sigma(I)$). The molecular structure is shown in Figure 2, along with a partial numbering scheme. Selected bond lengths and bond angles are given in Table 1. Fractional coordinates and additional crystallographic data can be found in the Supporting Information.

Structure Determination of PtMe$_2$(*rac*-1). Single crystals were grown by slow evaporation of acetone-d_6 in a warm water bath. The crystal data are summarized in the Supporting Information.

A total of 30 607 reflections with 2θ < 57° was collected on a Siemens P4/CCD diffractometer using graphite-monochromated Mo Kα radiation.[35,36] The structure was solved by direct methods and refined by full-matrix least squares on F^2 values with hydrogens riding.[37] Non-hydrogen atoms were refined with anisotropic displacement parameters. The final R and R_w factors were 0.0388 and 0.1014, respectively, for 10 615 reflections (I < $2\sigma(I)$).

Reaction of Allylammonium Triflate with *rac*-1 (Scheme 4). The reaction was carried out in an NMR tube. Solid allylammonium triflate (6.1 mg, 0.029 mmol) was added into a solution of *rac*-1 (21.5 mg, 0.025 mmol) in 1 mL of CD$_2$-Cl$_2$. The reaction was left for $^1/_2$ h. Allylammonium triflate only dissolves in CD$_2$Cl$_2$ upon reaction. Data: ^{1}H NMR spectrum shows a mixture of the free crown ether and the amine of Scheme 4; ^{1}H NMR (CDCl$_3$) of the free crown ether and the amine δ 1.57 (d, J = 6.80 Hz, 3H, CHCH_3 of amine), 3.03 (two AB quartets of ABX pattern, J = 13, 7.5, 5.3 Hz, 2H, NCH_2-CH=CH$_2$ of amine), 3.21 (t, J = 5.15 Hz, 2H, H$_2$NCH_2 of crown ether), 3.6−3.7 (m, 8H, CH_2CH_2OCH_2CH_2 of crown ether), 3.77 (m, 2H, H$_2$NCH$_2$CH_2 of crown ether and 3H of C$_5$H$_4$ or C$_5$H$_3$ of amine), 3.82 (m, 2H, PhOCH$_2$CH_2 of crown ether), 4.08 (m, 2H, PhOCH_2 of crown ether), 4.16 (m, 1H, C$_5$H$_4$ or C$_5$H$_3$ of amine), 4.25 (m, 1H, C$_5$H$_4$ or C$_5$H$_3$ of amine), 4.36 (m, 1H, HNCHCH$_3$), 4.46 (m, 1H, C$_5$H$_4$ or C$_5$H$_3$ of amine), 4.56 (m, 1H, C$_5$H$_4$ or C$_5$H$_3$ of amine), 4.89 (d, J = 17 Hz, CH_2=CH of amine), 5.00 (d, J = 10 Hz, CH_2=CH of amine), 5.2 (m, 1H, HNCH$_2$CH=CH$_2$), 6.58 (dd, J = 7.7, 1.3 Hz, 1H, PhH of crown ether), 6.63 (td, J = 7.5, 1.5 Hz, 1H, Ph H of crown ether), 6.77 (dd, J = 7.9, 1.4 Hz, 1H, Ph H of crown ether), 6.86 (td, J = 7.7, 1.5 Hz, 1H, Ph H of crown ether), 7.0−7.8 (m, 20H, Ph H of amine); ^{31}P NMR (CDCl$_3$) δ −16.3 (s, (C$_6$H$_5$)$_2$$P$), −25.7 (s, (C$_6H_5$)$_2$$P$) (^{31}P NMR (CDCl$_3$) of *rac*-1 δ −23.9 (s, (C$_6$H$_5$)$_2$$P$), 75.5 (s, (C$_6H_5$)$_2$$P$)).

Reaction of [Rh(NBD)$_2$]OTf and *rac*-1. A solution of *rac*-1 (9.9 mg, 1.2 × 10^{-2} mmol) in 0.5 mL of d_6-acetone was added dropwise to a solution of [Rh(NBD)$_2$]OTf (5.2 mg, 1.2 × 10^{-2} mmol) in 0.5 mL of d_6-acetone under nitrogen, resulting in a red solution. The product could not be isolated. Data: ^{1}H NMR (acetone-d_6) δ 1.47 (d, J = 6.9 Hz, 3H, CHCH_3), 1.56 (m, 2H, NBD CH_2), 3.16 (m, 1H, CH_2N), 3.41−3.83 (m, 10H, OCH_2CH_2), 3.87 (m, 2H, CH_2CH$_2$OPh), 3.91 (m, 1H, OCH_2), 4.05 (m, 2H, NBD CH), 4.10 (m, 1H, NBD vinyl H), 4.20 (m,

2H, CH_2OPh), 4.22 (m, 1H, Cp H), 4.27 (m, 1H, Cp H), 4.46 (m, 2H, Cp H), 4.54 (m, 1H, NBD vinyl$H$), 4.56 (m, 2H, Cp H), 4.79 (m, 2H, NBD vinyl H and Cp H), 4.90 (m, 1H, NBD vinyl H), 5.14 (q, J = 6.9 Hz, 1H, CHCH$_3$), 6.95 (m, 1H, NC$_6$H$_4$O), 7.00 (m, 2H, NC$_6$H$_4$O), 7.08 (m, 1H, NC$_6$H$_4$O), 7.37−8.14 (m, 20H, P(C$_6$H$_5$)$_2$); ^{31}P NMR (d_6-acetone) δ 29.7 (dd, J_{P-Rh} = 160 Hz, J_{P-P} = 26 Hz), 26.6 (dd, J_{P-Rh} = 162 Hz, J_{P-P} = 26 Hz).

Hydrogenation of MAC. All hydrogenations were performed with a gas uptake apparatus. A typical experiment was as follows: a 4 mL solution of 1:1 [Rh(NBD)$_2$]OTf and **1** or BPPFA (2.55 × 10^{-4} M) and 400 equiv of MAC in freshly distilled THF were added to a round-bottom flask. Three freeze−pump−thaw cycles were effected, and the solution was allowed to equilibrate to 25 °C while being stirred for 10 min. The gas was allowed to equilibrate with the solvent at 25 °C for 1 min, and the uptake of gas was monitored over a period of about 1 h. Upon exposure to hydrogen (700 Torr) the solution changed from yellow to orange-red.

Kinetic Studies of NBD Rotation of [Rh(NBD)(*rac*-1)]-OTf (9). A 13 mM solution of **9** was prepared in acetone-d_6. Kinetic experiments were performed on a Varian Inova 500 MHz spectrometer equipped with a pulsed field gradient unit and a triple-resonance (^{1}H−^{13}C−X) probe with an actively shielded z gradient. The relaxation delay was set to 2 s. The 1D DPFGSE-NOE spectra were collected at 25, 35, 45, 55, 65, 75, 85, 95, 105, 115, 125, 135, 145, 155, 165, 175, 185, 195, 205, and 215 ms mixing time and at 1, 6, 11, 16, 21, 26, 31, and 36 °C. Each spectrum was collected with eight scans. The vinyl NBD resonance at 4.9 ppm was selected for excitation. Integrated intensities were used for kinetic calculations. The simplex algorithm of Microsoft Excel was used to fit eqs 1 and 2, where I_1 and I_2 are integrated intensities of the excited peak and the corresponding peak, respectively, A is half of the empirical integrated intensity at t = 0, k is the rate constant, t is the mixing time, and R_1 and R_2 are spin−lattice relaxation rates of the excited peak and its exchange partner, respectively.

$$I_1 = A(1 + \exp(-2kt))(\exp(-R_1t)) \qquad (1)$$

$$I_2 = A(1 - \exp(-2kt))(\exp(-R_2t)) \qquad (2)$$

Determination of the Solution Structure of [Rh(NBD)-(*rac*-1)]OTf (9). A 13 mM solution of [Rh(NBD)(*rac*-1)]OTf (**9**) was prepared in acetone-d_6. All 2DNOESY data sets were acquired at 24 °C on a Varian UNITY 500 MHz spectrometer.

^{1}H DQF-COSY NMR Experiments. The spectrum was measured using a phase sensitive DQF-COSY pulse sequence[38,39] with an initial homospoil pulse and States−Haberkorn−Ruben phase cycling[40] at 24 °C. A total of 512 increments of 8 scans was collected with 2048 real points in t_2. The relaxation delay was set to 2.3 s. The FELIX NMR software package was used to transform and process data. The t_1 dimension was zero-filled to 1024 points, and the t_2 dimension was zero-filled to 4096 points. A linear prediction scheme was used to correct the first point and generate points at the tails of the FID, extending data by one-third. Gaussian line broadening and a skewed sine-squared bell function were applied to the FID.

^{1}H NOESY NMR Experiments. Spectra were collected at 300, 450, 600, 900, and 1200 ms mixing time using a phase-sensitive NOESY pulse sequence[41] with an initial homospoil pulse and States−Haberkorn−Ruben phase cycling.[40] Spectra were obtained at 24 °C in acetone-d_6. A total of 512 increments

(35) *SMART Software Reference Manual*; Siemens Analytical X-ray Instruments: Madison, WI 53719-1173, 1994.

(36) *SMART Software Reference Manual*; Siemens Analytical X-ray Instruments: Madison, WI 53719-1173, 1995.

(37) Sheldrick, G. M. *SHELXTL VERSION 5 Software Manual*; Siemens Analytical X-ray Instruments: Madison, WI 53719-1173, 1995.

(38) Piantini, U.; Sorensen, O. W.; Ernst, R. R. *J. Am. Chem. Soc.* **1982**, *104*, 6800.

(39) Rance, M.; Sorenson, O. W.; Bodenhausen, G.; Wagner, G.; Ernst, R. R.; Wuthrich, K. *Biochem. Biophys. Res. Commun.* **1983**, *117*, 479.

(40) States, D. J.; Haberkorn, R. A.; Ruben, D. J. *J. Magn. Reson.* **1982**, *48*, 286.

(41) Macura, S.; Ernst, R. R. *Mol. Phys.* **1980**, *41*, 95.

of 8 scans was collected with 2048 real points in t_2. The relaxation delay was set to 2.3 s. The FELIX NMR software package was used to transform and process data. The t_1 dimension was zero-filled to 1024 points, and the t_2 dimension was zero-filled to 4096 points. A linear prediction scheme was used to correct the first point and generate points at the tails of the FID, extending the data by one-third. A Kaiser window function and exponential line broadening were applied to the FID to reduce apodization artifacts. Low-order polynomial baseline corrections were applied to each dimension. The baselines were corrected again using FACELIFT from the National Magnetic Resonance Facility at Madison, WI, and the deconvolution facility in the FELIX program. Diagonal peak volumes at zero mixing times were estimated by fitting the observed diagonal peaks to an exponential function. For off-diagonal peaks, the intensities of the two symmetry-related peaks were averaged prior to normalization. Random numbers spanning the estimated noise level were generated and used to represent the intensities of "unseen" cross-peaks.

Generation of Static Model Conformers. The trial structures, totalling 343 conformers, were generated by conformer searching using CERIUS² and the Universal force field (UFF). Atom type Fe2+2 was introduced for Fe in the ferrocenyl group, and a harmonic angle constraint for the Cp−Fe−Cp angle (force constant = 1000 kcal/mol Å) was applied to prevent large distortions of the ferrocene during the searching. The starting conformer was adapted from the X-ray structure of **8a** and was well-minimized to a gradient RMS of 0.01 kcal/mol Å. Two torsion angles (Me−C35−N37−C_{ipso} and C15(Fc)−C14(Fc)−C35−Me) were systematically varied over 360° in the conformer searching. Hundreds of energy minimized conformers were obtained. Application of clustering algorithms reduced the number of conformers to 343 unique structures. The energy of each conformer was measured with the electrostatic term turned off.

Conformer Population Analysis of the Static Ensemble. Conformer population analysis proceeds by computing the full NOE time course for each conformer in the trial set and then finding the most parsimonious set of conformers that best reproduce the observed data. The 2DCPA program was modified to accommodate the chemical exchange process according to a two-site exchange model. Known distances between pairs of protons (bridge CH_2−bridgehead CH of norbornadiene and some *ortho−meta* and *meta−para* phenyl protons) were used for calibration of the rotational correlation time (τ_1 = 0.2549 ns). The static ensemble was exhaustively fitted with each possible single, double, and triple conformer in solution according to a fast conformer exchange model. Significance testing was performed using Hamilton's F test on every possible combination of the 10 best fits of the singles, doubles, and triples.

The populations obtained by 2DCPA depend on the relative weightings of the NOE data. In particular, the extent to which reproduction of absent NOE peaks is included in the data analysis dramatically effects the absolute value of the R factor (and may influence relative conformer populations). A subset (296 data points) of the 496 total points was treated as absent peaks. The contribution of absent peaks to the error function was calculated as $(I^{calcd} - I^{obsd})^2/100$. For all other peaks, the contribution to the error function was $(I^{calcd} - I^{obsd})^2$.

The best single-conformer fit to the data exhibits the R factor 0.896. The best double-conformer fitting shows the lowest R factor (R = 0.868) with fractional populations of 0.61 and 0.39, while the three-conformer fitting yields an R factor of 0.857 with fractional populations of 0.54, 0.33, and 0.13. Application of the F test at the 95% confidence level, excluding the absent peak data points, indicates that it is statistically significant to use three rather two or one conformers in fitting the data but that four conformations do not lead to a significantly better fit relative to three conformations.

Supporting Information Available: Crystallographic data for PtMeI(*rac*-**1**) and PtMe₂(*rac*-**1**), NMR spectra of **8** and **9**, and input files and results pertaining to the 2DCPA analysis of solution NOE data. This material is available free of charge via the Internet at http://pubs.acs.org.

OM990391U